Title

Phase Separation, Reaction Equilibrium, and Self-Assembly in Binary Telechelic Homopolymer Blends.

Journal

Macromolecules, 56(24)

ISSN

0024-9297

Authors

Vigil, Daniel
Zhang, Amy
Delaney, Kris
et al.

Publication Date

2023-12-26

DOI

10.1021/acs.macromol.3c01653

Peer reviewed

Macromolecules

pubs.acs.org/Macromolecules
Article

Phase Separation, Reaction Equilibrium, and Self-Assembly in Binary Telechelic Homopolymer Blends

Daniel L. Vigil, Amy Zhang, Kris T. Delaney, and Glenn H. Fredrickson*

Cite This: *Macromolecules* 2023, 56, 9994−10005
Read Online

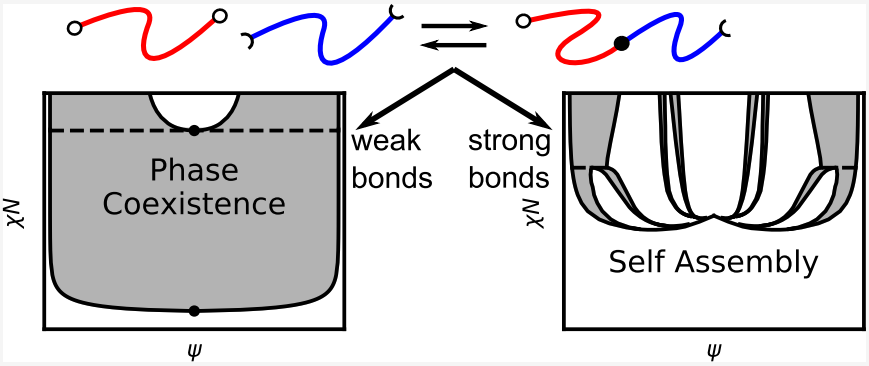

ABSTRACT: We study a binary blend of telechelic homopolymers that can form reversible AB-type bonds at the chain ends. Reversibly bonding polymers display novel material properties, including thermal tunability and self-healing, that are not found in conventional covalently bonded polymers. Previous studies of reversibly bonding polymer systems have been limited by the computational demand of accounting for an infinite number of possible reaction products in a spatially inhomogeneous, self-assembled structure. We demonstrate that newly developed theoretical models and numerical methods enable the simultaneous computation of phase equilibrium, reaction equilibrium, and self-assembly via self-consistent field theory. Phase diagrams are computed at a variety of physically relevant conditions and are compared with nonreactive analogues as well as previous experimental studies of telechelic polymer blends.

INTRODUCTION

Block copolymers (BCPs) are a major industrial platform due to their highly tunable properties via self-assembly and the ability to compatibilize dissimilar polymers. A major triumph of polymer physics is the ability to predict when melts and solutions of homopolymers and copolymers will mix into a single liquid, macroscopically phase separate into two liquids,[1,2] or self-assemble into a solid-like microstructure.[3] One important tool for predicting this phase behavior is numerical self-consistent field theory (SCFT), which is particularly effective at computing the free energies of the self-assembled microstructures.[4] Numerical advances over the last 30 years have enabled efficient simulation of complex self-assembled structures, including Frank−Kasper sphere phases.[5,6] The standard approach for numerical SCFT uses an auxiliary field (AF)-based model, which decouples chain interactions via a set of local potential fields.[4] This approach is well suited to polymer systems with a predefined distribution of components in the mixture or "quenched" systems.[7] In recent years, however, there has been significant interest in supramolecular interactions, where polymers and small molecules can form and dissociate bonds reversibly and are in a dynamic equilibrium. These types of interactions appear in both synthetic and biological polymers, including intrinsically disordered proteins[8] and polymers functionalized with acid and base groups,[9,10] multiple hydrogen bonds,[11] and ligands that bind to metals.[12] Supramolecular interactions are also of industrial interest as some commodity polymers, such as thermoplastic polyurethanes, can reversibly dissociate and form bonds at elevated temperatures.[13−15] Supramolecular interactions can also lead to exotic phase behavior, including reentrant phase transitions,[16] and can also be leveraged to make thermally tunable[10] and self-healing materials.[17]

Some authors have studied supramolecular polymer systems with theories similar to those of AF-SCFT by coupling the theories to analytical approximations. In particular, the phase

Received: August 18, 2023
Revised: October 30, 2023
Accepted: November 28, 2023
Published: December 13, 2023

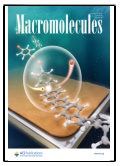

https://doi.org/10.1021/acs.macromol.3c01653
Macromolecules 2023, 56, 9994−10005

separation and gelation of blends of linear polymers with associating groups along the length of the polymer have been studied by multiple groups.[18−21] These analytical approaches have not been used to examine the microstructures formed during self-assembly, however, even though theory and experiments[9,16,22−24] show that self-assembly occurs in supramolecular polymer blends. One group of authors used molecular dynamics simulations to examine microphases and were able to study domain sizes, but they did not create comprehensive phase diagrams.[19]

There have been attempts to extend the numerical AF-SCFT approach to supramolecular polymers.[25−29] For systems in which only a finite set of products can be formed, the approach works well, and phase diagrams that include microphases have been computed. One example is a supra-diblock system in which two dissimilar homopolymers each have one functional group on a chain end that can link together to form a diblock.[26] In many systems, however, there are an unlimited number of possible products. This includes telechelic and network-forming polymers. For these systems with an unlimited set of products, the AF-SCFT approach relies on generating functionals to enumerate the linear and tree-like products, but neglects ring and loop products.[28] Even with these approximations, the approach is limited by the computational expense of numerically solving integral equations inside the SCFT field iteration and has not been widely deployed. In particular, comprehensive phase diagrams have not been developed for any system with an unlimited set of reaction products.[29]

Recent theoretical developments have produced an alternative to the AF approach that instead represents polymers via coherent state (CS) fields.[30,31] These CS models are particularly effective for supramolecular systems as they can represent all possible reaction products with the proper weighting, even when there are an unlimited number of products.[32] The models are of finite order in the CS fields and do not rely on any approximate scheme for partially summing product contributions. Recent numerical advances have enabled efficient simulation of these models as well,[33] though these algorithms have not yet been applied to supramolecular polymers.

In this work, we combine these theoretical and numerical advances to demonstrate that CS-SCFT can be used to construct full phase diagrams incorporating reaction equilibrium for supramolecular polymers. As a model system, we consider a binary blend of telechelic homopolymers that can form AB-type bonds. This system can form arbitrarily long alternating AB-type BCPs, which makes it intractable to AF-SCFT calculations. The full CS theory also accounts for ring polymers that can be formed, but the mean field approximation invoked for SCFT does not enumerate these products.[34] We compute full phase diagrams that include phase coexistence between disordered phases and microphases, including the body-centered cubic (BCC) sphere phase and the double gyroid network phase (GYR). These phases require 3D calculations, which have not been performed for supramolecular BCPs with infinite product sets before.

With our approach, we are able to demonstrate three different regimes of phase behavior depending on the relative strength of the bond equilibrium and the phase segregation strength. When bonds are weak, the system behaves similarly to a nonreactive homopolymer blend. In the opposite limit, when bonds are strong, the system behaves like a pure BCP melt or BCP-homopolymer blend, depending on the stoichiometry of the system. In the intermediate regime, we observe a complex interplay between macroscopic phase separation and microphase segregation characteristic of the region around a Lifshitz point. In addition to phase diagrams, we are able to predict the reaction equilibrium in the system as well as the microphase structure, including domain spacing. These results demonstrate the range of possible phase behavior and will help guide experimental polymer chemists who use supramolecular chemistry in polymer blends.

MODEL AND METHODS

We consider a binary melt blend of A and B telechelic homopolymers in which each A-type chain end can reversibly bind to a single chain end of type B (heterobonding motif). A CS model for such a system in the canonical ensemble is

$$Z = Z_0 \int \mathcal{D}w_+ \int \mathcal{D}w_- \int \mathcal{D}(\phi_A, \phi_A^*) \int \mathcal{D}(\phi_B, \phi_B^*) \, e^{-H[w_+, w_-, \phi_A, \phi_A^*, \phi_B, \phi_B^*]} \tag{1}$$

$$H = \frac{\rho_0}{\chi} \int d\mathbf{r} \, (w_-(\mathbf{r}))^2 - \rho_0 \int d\mathbf{r} \, w_+(\mathbf{r}) - \sum_{K \in \{A,B\}} n_K \ln\left(\frac{1}{V} \int d\mathbf{r} \, (\phi_K^*(\mathbf{r},0))^2 \right) + \sum_{K \in \{A,B\}} \int ds \int d\mathbf{r} \, \phi_K^*(\mathbf{r}, s) \left(\partial_s - \frac{b_K^2}{6} \nabla^2 + w_K(s) \right) \phi_K(\mathbf{r}, s) - \sum_{K \in \{A,B\}} \int d\mathbf{r} \, \phi_K\left(\mathbf{r}, \frac{N_K}{2}\right) - \frac{K_b}{\rho_0} \int d\mathbf{r} \, \phi_A\left(\mathbf{r}, \frac{N_A}{2}\right) \phi_B\left(\mathbf{r}, \frac{N_B}{2}\right) \tag{2}$$

Here, Z is the partition function, Z_0 is the ideal gas partition function, and H is the effective Hamiltonian. Normalizing denominators for the functional integrals have been absorbed into Z_0.[31] The Hamiltonian depends on four CS fields (φ_A, φ_A^*, φ_B, and φ_B^*) and two AFs (w_+ and w_-), so the model may be referred to as a hybrid AF-CS model. The AFs are defined over all of space $\mathbf{r}$, whereas the CS fields depend on $\mathbf{r}$ as well as the chain contour position, $s \in [0, N_K/2]$. Each term in the Hamiltonian has a simple physical interpretation. The logarithmic terms on the second line create the appropriate number of homopolymer precursor chains, n_A or n_B, depending on species. The terms contain factors of $(\varphi^*(\mathbf{r},0))^2$, which creates two polymer arms at a core $s = 0$ contour position. The third line of the Hamiltonian is responsible for propagating these arms outward from the core in s using the appropriate chain statistics. In this work, we consider flexible continuous Gaussian chains, which leads to the diffusive-type operator $\partial_s - \nabla^2$ that appears in the Hamiltonian. The statistical segment length can be set for each species via b_K, but we consider only $b_A = b_B = 1$ in this work. While an arm is being propagated, it experiences the relevant species potential field w_A or w_B, which are related to the $w_\pm$ AFs via a simple linear transformation

$$w_A = w_+ - w_- \tag{3}$$

$$w_B = w_+ + w_- \tag{4}$$

An important feature of the model is that the integration path of w_- is over real values, while w_+ is pure imaginary. The species fields w_A and w_B are thus complex-valued, as is the Hamiltonian. After $N_K/2$ segments, the arm is terminated via the first term in the last line. Because the polymer was initialized as a star with two arms, this creates a linear chain with a total length of N_K. Unless otherwise specified, we choose the following equation: $N_A = N_B$. The final term in the Hamiltonian enables an A and a B polymer to link together at their chain ends and has an associated equilibrium constant K_b. In addition to creating the diblock, this term also creates all higher-order products, including triblock, tetrablock, and so on. Finally, the first two terms in the model represent the nonbonded interactions

https://doi.org/10.1021/acs.macromol.3c01653
Macromolecules 2023, 56, 9994−10005

between polymer segments in the model. The first introduces a Flory–Huggins interaction between A and B segments parametrized by χ and the second enforces incompressibility at a segment number density $\rho_0 = (n_A N_A + n_B N_B)/V$, where V is the total volume of the system and n_K is the number of species K telechelic polymers.

It is possible to remove the AFs by explicit evaluation of the $w_\pm$ integrals, resulting in a "pure" CS model with additional interaction terms that are fourth order in the CS fields.[30,32] However, previous work has found the hybrid representation more amenable to numerical simulation so we retain this form of the model for the present study.[33] Although we have presented the model here based on physical arguments, it is possible to derive it rigorously from an AF model, as is demonstrated in the literature.[30,31] Correspondingly, it is possible to show that every copolymer product, both linear and cyclic, is accounted for correctly by performing a perturbation expansion in the powers of K_b.

It is worth discussing the relationship between the model parameters and the parameters under experimental control. In the model, polymer segments are defined to have equal volume, so the volume fraction of a given segment type (A or B) is $\psi_K = n_K N_K/(n_A N_A + n_B N_B)$. Two model parameters have important temperature dependences: χ and K_b. For most polymer pairs, the chi parameter can typically be fitted to an expression of the form

$$\chi = C_1 + C_2/T \tag{5}$$

where T is temperature and C_1 and C_2 are constants that may depend on the composition ψ_A of the blend.

The equilibrium constant follows the relation

$$K_b = \exp\left(\frac{\epsilon_b - s_b T}{k_B T}\right) \tag{6}$$

where k_B is Boltzmann's constant, ϵ_b is the enthalpy of reaction, and s_b is the entropy of reaction. We assume for simplicity that both ϵ_b and s_b are independent of temperature.

The model presented above can be applied to any experimental system for which there is a known temperature dependence for χ and K_b. In this work, rather than specializing on specific chemistries, we make an approximation to examine general trends. We assume that χ is inversely proportional to temperature ($C_1 = 0$ in eq 5) and that the entropy of reaction $s_b = 0$. With these approximations, χ and $h = \ln(K_b)$ are both inversely proportional to temperature and their ratio is independent of temperature. This allows us to use χ as an inverse temperature scale and h/χ as a chemistry-dependent property that represents the strength of bonding compared to phase separation.[26,27]

As a final note, it is conventional in unreactive BCPs to specify χN rather than χ as it is the combined grouping that controls the phase behavior for linear chains. This is no longer true in the telechelic model considered here, as the reaction can only occur at end groups. Changing N_A or N_B changes the concentration of these end groups, breaking the universal phase behavior for a fixed χN. Nevertheless, to match convention, we will use the combined grouping χN_A and $h/\chi N_A$ and fix $N_A = 100$. Although this reduces the generality of the results presented here, it is well understood how changing N affects phase behavior and reaction equilibrium based on previous literature results.[26]

We now turn to physical observables that can be computed by field operators. The first of these is the segment density of the A or B species

$$\tilde{\rho}_K(\mathbf{r}) = \int \mathrm{d}s\, \varphi_K^*(\mathbf{r}, s)\varphi_K(\mathbf{r}, s) \tag{7}$$

a similar quantity that only considers the unreacted end segments of a chain can also be defined as an end density

$$\tilde{\rho}_{K,e}(\mathbf{r}) = \varphi_K(\mathbf{r}, N_K/2) \tag{8}$$

Finally, an operator for the local density of bonds is defined via

$$\tilde{\rho}_b(\mathbf{r}) = \varphi_A(\mathbf{r}, N_A/2)\varphi_B(\mathbf{r}, N_B/2) \tag{9}$$

These operators give important information about the spatial distribution of the segments in the system. We are also concerned with bulk properties as well, including the total number of bonds

$$n_b = \left\langle \int \mathrm{d}\mathbf{r}\, \varphi_A(\mathbf{r}, N_A/2)\varphi_B(\mathbf{r}, N_B/2) \right\rangle \tag{10}$$

and number of unreacted ends of a given species in the system

$$n_{K,e} = \left\langle \int \mathrm{d}\mathbf{r}\, \varphi_K(\mathbf{r}, N_K/2) \right\rangle \tag{11}$$

Here, the angle brackets denote an average over field configurations. Another useful quantity is the conversion of end groups, which is defined as

$$\alpha_K = \frac{2n_K - n_{K,e}}{2n_K} = \frac{n_b}{2n_K} \tag{12}$$

The conversion of end groups for species A and B is related because only AB-type bonds can form

$$\frac{\alpha_A \psi_A}{N_A} = \frac{\alpha_B \psi_B}{N_B} \tag{13}$$

The internal stress of a blend can also be computed via a field operator. Such an operator is familiar in AF representations and has a similar form in the CS model. The full derivation of such an operator can be found in the Supporting Information of a recent publication by Fredrickson and Delaney,[35] so we present the final result

$$\tilde{\boldsymbol{\sigma}} = \sum_{K\in\{A,B\}} \frac{k_B T b_K^2}{3V} \int \mathrm{d}\mathbf{r} \int \mathrm{d}s\, \varphi_K(\mathbf{r}, s)\nabla\nabla\varphi_K^*(\mathbf{r}, s) \tag{14}$$

A final important operator is the chemical potential, which is required to construct phase-coexistence regions. For a given species, the excess chemical potential in units of the thermal energy $k_B T$ is

$$\mu_{K,ex} = -\ln\left(\frac{1}{V}\int \mathrm{d}\mathbf{r}\, (\varphi_K^*(\mathbf{r},0))^2\right) \tag{15}$$

This chemical potential is in excess of the ideal gas chemical potential of a non-interacting reference system with no supramolecular bonds.

The previously discussed operators give average information about the reaction equilibrium, such as the conversion, but we would also like to know the distribution of products in the system, including how much of each type of BCP is formed. Unfortunately, there is no known operator using the CS fields that can be used to compute the number of each type of reaction product. It is possible, however, to compute the number of chains of a given species in an AF model formulated in the grand canonical ensemble. Although the unlimited number of reaction products makes it intractable to use the AF model to establish reaction equilibrium, we can use the CS model to obtain equilibrium field configurations and then evaluate operators in the AF model to quantify the number of any individual reaction product. The effective Hamiltonian for an AF model of the telechelic blend presented here is

$$\begin{aligned} H_{AF}[w_+, w_-] &= \frac{\rho_0}{\chi}\int \mathrm{d}\mathbf{r}\, (w_-(\mathbf{r}))^2 - \rho_0 \int \mathrm{d}\mathbf{r}\, w_+(\mathbf{r}) \\ &\quad - \sum_{j=1}^{\infty} z_{A_jB_j} V Q_{A_jB_j}[w_+, w_-] \\ &\quad - \sum_{j=1}^{\infty} (z_{A_jB_{j-1}} V Q_{A_jB_{j-1}}[w_+, w_-] + z_{A_{j-1}B_j} V Q_{A_{j-1}B_j}[w_+, w_-]) \\ &\quad - \sum_{j=1}^{\infty} (z_{A_jB_j,\mathrm{ring}} V Q_{A_jB_j,\mathrm{ring}}[w_+, w_-]) \end{aligned} \tag{16}$$

https://doi.org/10.1021/acs.macromol.3c01653
Macromolecules 2023, 56, 9994−10005

and the number of each product can be computed via

$$n_{A_jB_k} = \left\langle z_{A_jB_k} V Q_{A_jB_k}[w_+, w_-] \right\rangle \tag{17}$$

The first two terms of the effective Hamiltonian are equivalent to those of the CS model and represent Flory interactions and incompressibility. The remaining terms contain activities z and single-chain partition functions $Q[w_+, w_-]$ for all the possible products that can be formed. The activities and single-chain partition functions can also be used to compute the number of each product. The products can be classified into three types: linear chains that are composed of an equal number of A and B chains and are terminated by one A chain and one B chain, linear chains with one excess A or B chain that are doubly A or B terminated, and ring polymers, which must have an equal number of A and B chains. One can demonstrate that the activity of each type of chain can be related to the activity of the A and B homopolymers, z_A and z_B, and the equilibrium constant K_b via

$$z_{A_iB_j} = \begin{cases} (2z_A)^i (2z_B)^j \left(\dfrac{K_b}{\rho_0}\right)^{i+j-1} & i = j, \text{ linear} \\ \dfrac{1}{2}(2z_A)^i (2z_B)^j \left(\dfrac{K_b}{\rho_0}\right)^{i+j-1} & |i-j|=1 \\ \dfrac{1}{2j}(2z_A)^i (2z_B)^j \left(\dfrac{K_b}{\rho_0}\right)^{i+j} & i = j, \text{ ring} \end{cases} \tag{18}$$

the cases of this equation represent the different types of products, as discussed previously. The first two cases, which represent different types of linear chains, are nearly identical, only differing by a factor of 2. The products that are doubly A terminated or doubly B terminated are head−tail symmetric so their activity carries a factor of 1/2 to account for this degeneracy. Similarly, for ring polymers, there is a factor of $1/2j$ that accounts for the rotational symmetry of the molecule. There is also an additional factor of K_b that accounts for the extra supramolecular bond in a ring compared with a linear chain.

Although we have expressions for the activities of each product, we still require the activities of the homopolymers and also the values of the single-chain partition functions to compute the number of each product. The homopolymer activities can be computed from the chemical potential determined from canonical ensemble simulations with the CS model since $z_A = \rho_0 \exp(\mu_A)$. All that remains then is to compute the ensemble average single-chain partition function value for each chain using equilibrium field configurations from the CS simulation. This would normally be prohibitively expensive since there are an infinite number of reaction products. We circumvent this issue by considering only BCPs containing up to 14 telechelic homopolymers. We note that the equilibrium field configurations obtained from the CS simulation account for all products, not just those considered in the truncated set. One can evaluate how much of the mass is accounted for with the truncated set of products by comparing the total number of polymers from the original CS canonical simulation and comparing it to the number of products computed from the AF approach. In all cases in this work, the truncation error is less than half a percent, unless otherwise noted. The truncated set can also be extended to larger products if it is found to be missing a significant fraction of the polymer mass.

The distribution calculation in this work is further accelerated by the fact that we limit ourselves to SCFT calculations and must evaluate each Q only at the final mean-field (saddle point) configuration obtained from the CS model. We discuss details of the numerical SCFT method in the following section. For the disordered phase, numerical simulations are not required and the single-chain partition function can be computed analytically under SCFT. Additionally, in the disordered phase, the activity of the A and B homopolymers can be related to the system composition analytically. We can then analytically compute the distribution of products in the disordered phase, which yields

$$\alpha_K = \frac{1 + \frac{1}{2}K_b\left(\frac{\psi_A}{N_A} + \frac{\psi_B}{N_B}\right) - \sqrt{1 + K_b\left(\frac{\psi_A}{N_A} + \frac{\psi_B}{N_B}\right) + \frac{1}{4}K_b^2\left(\frac{\psi_A}{N_A} - \frac{\psi_B}{N_B}\right)^2}}{\frac{\psi_K}{N_K}K_b} \tag{19}$$

$$\psi_{A_jB_{j-1}} = (1-\alpha_A)^2(\alpha_A\alpha_B)^{j-1}\psi_A\left(\frac{jN_A + (j-1)N_B}{N_A}\right) \tag{20}$$

$$\psi_{A_{j-1}B_j} = (1-\alpha_B)^2(\alpha_A\alpha_B)^{j-1}\psi_B\left(\frac{(j-1)N_A + jN_B}{N_B}\right) \tag{21}$$

$$\psi_{A_jB_j} = 2(1-\alpha_A)(1-\alpha_B)(\alpha_A\alpha_B)^{j-1}\alpha_A\psi_A\frac{N_A + N_B}{N_A} \tag{22}$$

Equation 19 gives the conversion of species A or B in the disordered phase, while eqs 20−22 provide expressions for the volume fractions of the different types of products that can be formed. The three types of products include A-terminated chains, B-terminated chains, and chains terminated with one A and one B telechelic. Note that SCFT does not account for rings. One can show analytically via an infinite summation that the volume fractions sum to unity, indicating that we have properly accounted for all products. The compositions are also consistent with a probabilistic interpretation of the product distribution. In the disordered state, the system is assumed to be well mixed, so the probability that an A chain end is reacted is α_A, and the probability that it is unreacted is $(1-\alpha_A)$. The probability that an A telechelic has two unreacted ends is then $(1-\alpha_A)^2$, which is proportional to the amount of unreacted homopolymer in the blend, consistent with eq 20. To form an AB diblock requires an A telechelic with one unreacted end and one reacted end, generating the weight $2\alpha_A(1-\alpha_A)$, where the factor of 2 accounts for the indistinguishability of the two ends. The reacted end must be linked to a B block, which then has its other end unreacted and is associated with a factor of $(1-\alpha_B)$. The volume fraction of an AB diblock should then be proportional to $2\alpha_A(1-\alpha_A)(1-\alpha_B)$, which is consistent with eq 22. One can extend this logic to higher-order products; for example, an ABA triblock has the expected factor of $(1-\alpha_A)^2\alpha_A\alpha_B$ and is properly accounted for in eq 20.

Numerical Self-Consistent Field Theory. Numerical SCFT is an approximation to the full model in which we only consider a single saddle point configuration that satisfies the equations

$$\frac{\delta H}{\delta w_\pm(\mathbf{r})} = \frac{\delta H}{\delta \varphi_K^*(\mathbf{r}, s)} = \frac{\delta H}{\delta \varphi_K(\mathbf{r}, s)} = 0 \tag{23}$$

The free energy of the system is equal to the value of the effective Hamiltonian evaluated in these saddle-point field configurations.

To obtain the saddle-point fields, we use a previously developed algorithm.[33] The simulations are conducted in orthorhombic unit cells with periodic boundary conditions. The phases considered in this work are disordered liquid (DIS), LAM, hexagonally packed cylinders (HEX), BCC spheres (BCC), and a GYR. It is possible that other phases, such as close-packed spheres or Frank−Kasper sphere packings may occur, but we do not consider them here. The 3D phases, BCC and GYR, were spatially discretized using a 64^3 mesh, while the 2D HEX phase was discretized with a 64 by 108 grid and the 1D LAM phase used 128 grid points. In all calculations, the polymer contour was discretized with 11 sample points on a Chebyshev grid across the interval $[0, N_K/2]$ for each polymer. The SCFT equations were nondimensionalized using $R_g = b(N_A/6)^{1/2}$ as a reference length scale and k_BT as an energy scale. All calculations were run until the L_2 norm of the first variation of the dimensionless Hamiltonian was less than 1×10^{-7} with respect to all fields. A

https://doi.org/10.1021/acs.macromol.3c01653
Macromolecules 2023, 56, 9994−10005

variable cell shape algorithm was employed to obtain stress-free configurations,[36] with stress quantified using a nondimensionalized version of the CS stress operator presented earlier. All calculations were run until the stress was less than 10^{-6}.

Gibbs Ensemble. For the blend system considered here, it is possible for the system to macroscopically separate into multiple coexisting phases. Although there are many possible products in the melt, all are formed from the two starting macromonomers via the reaction equilibrium. Thus, the only independent chemical potentials are those of the two telechelic homopolymers, and only two-phase coexistence regions are possible. This is in contrast to unreactive A homopolymer, B homopolymer, and diblock blends, which display three-phase coexistence.[37−40] To determine binodals of phase coexistence, we use the Gibbs ensemble approach pioneered by Panagiotopoulos in the context of particle simulations.[41,42] The Gibbs ensemble approach was later adapted to field theoretic simulations by Riggleman and co-workers[43] and eventually specialized to SCFT of incompressible blends by Mester and coauthors.[44,45] We employ the Gibbs ensemble method of Mester et al. in this work. In a Gibbs ensemble, the system is divided into two subsystems, with each containing a different phase. The temperature, number of polymers, and total volume of the system are fixed. We adjust the composition and volume of each subsystem to equalize the osmotic pressure and chemical potential between the two subsystems, subject to the mass and volume conservation constraints of the total system. This approach only requires one calculation per temperature along each binodal, in contrast to other approaches such as common tangent or grand canonical ensemble that require many calculations.[46]

RESULTS AND DISCUSSION

Weak Bonding. We first examine a case where bonding is weak compared to the tendency for phase separation and set $h/\chi N_A = 0.5$. Figure 1 shows the phase diagram in the space of

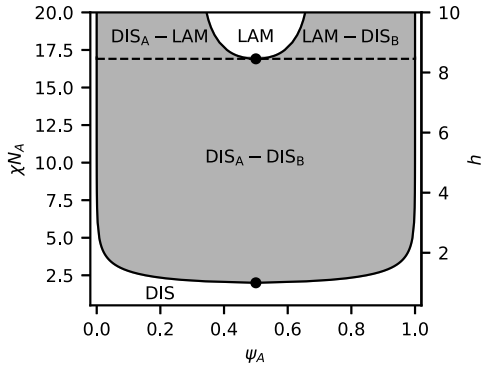

Figure 1. Phase diagram for a binary blend of heterobonding telechelic homopolymers at $h/\chi N_A = 0.5$. Shaded regions indicated two-phase coexistence, while white areas indicate a single-phase. Critical points are indicated with solid dots.

χN_A, which is inversely proportional to temperature, and the volume fraction of A segments ψ_A. The phase diagram is dominated by a region of phase coexistence between an A-rich DIS and a B-rich DIS. This is very reminiscent of an unreactive homopolymer binary blend, and the critical point in the reactive system is quite close to that of the unreactive system ($\chi N_A = 2.0$, $\psi_A = 0.5$). At sufficiently high χN_A, a region emerges where the lamellar phase is stable, which is flanked by regions of coexistence with disordered phases. Because the ratio of $h/\chi N_A$ is fixed, increasing χN_A also increases the equilibrium constant, favoring BCP product formation.

To better understand the phase behavior, it is useful to examine the reaction equilibrium in the blend. Figure 2 shows the conversion of species A as χN_A is varied at a fixed total

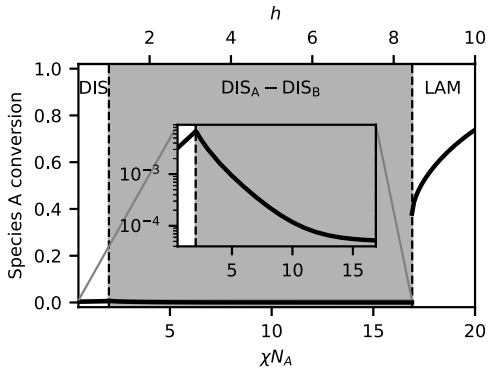

Figure 2. Species A conversion, α_A, versus χN_A (solid dark line), at $h/\chi N_A = 0.5$ and $\psi_A = 0.5$. Shading and text labels indicate the stable phase(s). Vertical dashed lines indicate phase boundaries. The inset shows an expanded view of the conversion for $\chi N_A < 16.9$ on a logarithmic y-axis.

composition of $\psi_A = 0.5$. Because the system is symmetric, at this composition $\alpha_A = \alpha_B$ and we plot only plot α_A. The inset of Figure 2 shows that below the critical point near $\chi N_A = 2$, the conversion is quite low ($O(10^{-3})$), but increases with increasing χN_A. This trend reverses at the critical point, however, and increasing χN_A decreases the conversion in the system until $\chi N_A = 16.9$. We attribute this to the increasing strength of phase segregation in this region. The conversion decreases because, as χN_A increases, there are fewer and fewer B chains present in the A-rich phase with which A chains can react, and vice versa. Finally, at $\chi N_A = 16.9$, the lamellar phase forms, and there is a sudden increase in the conversion. The equilibrium constant K_b has increased sufficiently that it is now energetically favorable to remix the two liquids so that they can form BCPs, which then self-assemble into a lamellar structure. There is still a significant amount of homopolymer in the mixture, but it can segregate to the interior of the A and B domains, while the BCPs act like surfactants at the interface.

Just past the critical point, the domain spacing of the lamellar phase is quite large (≈8 R_g) compared to a lamellar domain formed from pure AB diblocks of length $2N_A$ (5.5 R_g) at the same χN_A. For a volume fraction of A less than 0.35 or greater than 0.65, the system exhibits phase coexistence between the lamellar phase and a disordered phase. The disordered phase is composed almost entirely of the majority component of the system and contains almost purely homopolymers and almost no BCPs. Rather than swelling the lamellar domain with all the excess homopolymer that exists because of stoichiometry, it is instead favorable to eject it into a separate phase and maintain a less swollen lamellar phase. Because our calculations invoke a mean field approximation, there are no thermal fluctuations and Helfrich repulsions that would promote unbinding for highly swollen LAM, possibly leading to a microemulsion.[47,48]

Further increasing χN_A above 17 leads to further increased conversion and depletion of the remaining homopolymer in the system. This causes the domain size to decrease as there is less homopolymer to swell the system. We truncate this phase diagram at $\chi N_A = 20$, but it is possible that other phases can form at even higher values of χN_A. The conversion provides a simple scalar description of the reaction equilibrium but does not provide information on what types of BCPs are present in the system. In Figure 4, we plot the distribution of products at $\psi_A = 0.5$ and $\chi N_A = 17$ and $\chi N_A = 20$.

https://doi.org/10.1021/acs.macromol.3c01653
Macromolecules 2023, 56, 9994−10005

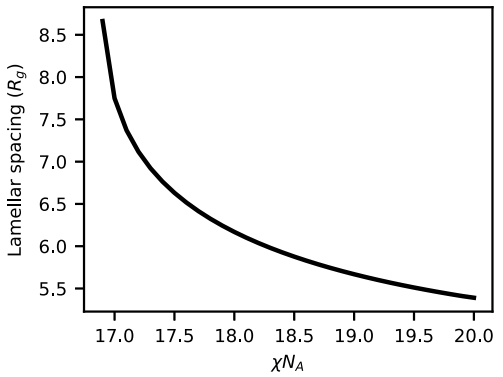

Figure 3. Domain spacing of the lamellar phase as a function of χN_A at $h/\chi N_A = 0.5$ and $\psi_A = 0.5$.

At $\chi N_A = 17$, the distribution is dominated by the AB diblock and the individual homopolymers, with triblocks and the tetrablock also making meaningful contributions to the total volume of the system. Higher order BCPs quickly become irrelevant with increasing size; however, at $\chi N_A = 20$, the distribution is significantly broadened and the amount of homopolymer is reduced by 80% compared to $\chi N_A = 17$. The average product is also shifted to longer BCPs. Note that the products considered in Figure 4 account for only 93% of the mass, the remainder of which is composed of longer BCPs not included in the population analysis. The dramatic increase in average polymer size upon changing χN_A from 17 to 20 may lead to significantly slowed dynamics in experimental systems and prevent the observation of equilibrium phases due to kinetic trapping.

Experimentally, there will also be ring polymers formed in the blend, although these are neglected by the mean field approximation of SCFT, as mentioned earlier. It is known that a melt of ring diblock copolymers has a larger value of χN_{ODT} than a melt of linear diblock copolymers.[49] Molecular dynamics simulations of blends of type A ring homopolymers and type B linear homopolymers show that the rings and linears undergo phase separation at larger values of χN compared to blends of linear homopolymers.[50] Together, these effects imply that including ring polymers in the blends produced by telechelic heterobonding homopolymers will likely stabilize the disordered phase and shift the ordered phase (LAM) window to larger values of χN_A.

Strong Bonding. We now consider a case where the equilibrium constant is large compared to the segregation strength and set $h/\chi N_A = 2$, the phase boundaries for which are plotted in Figure 5. Contrary to the weak-bonding case, there is no large coexistence region between disordered phases. Instead, the phase diagram is dominated by regions of microphases separated by channels of phase coexistence. At the edges of the phase diagram, there are significant regions of phase coexistence between the microphase and the disordered phase. Similar to the weak-bonding case, it is favorable to eject excess homopolymer to avoid significantly swelling the domains. It is also possible that other sphere phases, such as close-packed spheres or Frank−Kasper phases, could be present in these regions, but we do not consider them in this work. While the relative position of the stable region for each microphase is similar to that of unreactive BCPs, there are some notable differences, including the fact that the BCC phase becomes unstable above $\chi N_A \approx 10.5$ and is replaced with a two-phase window between DIS and HEX. The shape of the

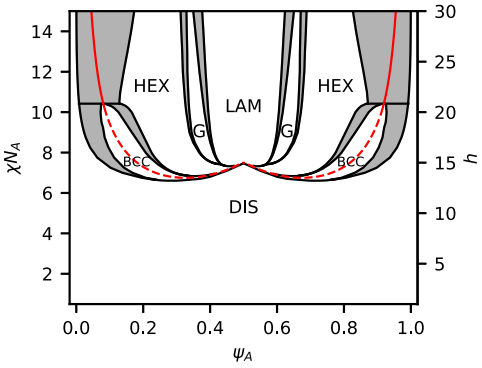

Figure 5. Phase diagram for a binary blend of heterobonding telechelic homopolymers at $h/\chi N_A = 2.0$. Shaded regions indicate two-phase coexistence, while white regions indicate a single-phase is present. The present phases are a homogeneous DIS, LAM, GYR, HEX, and BCC packing of spheres. Red line indicates the RPA spinodal boundary. Dashed segments indicate instability at the nonzero wave vector. Solid segments indicate instability at wave vector $k = 0$.

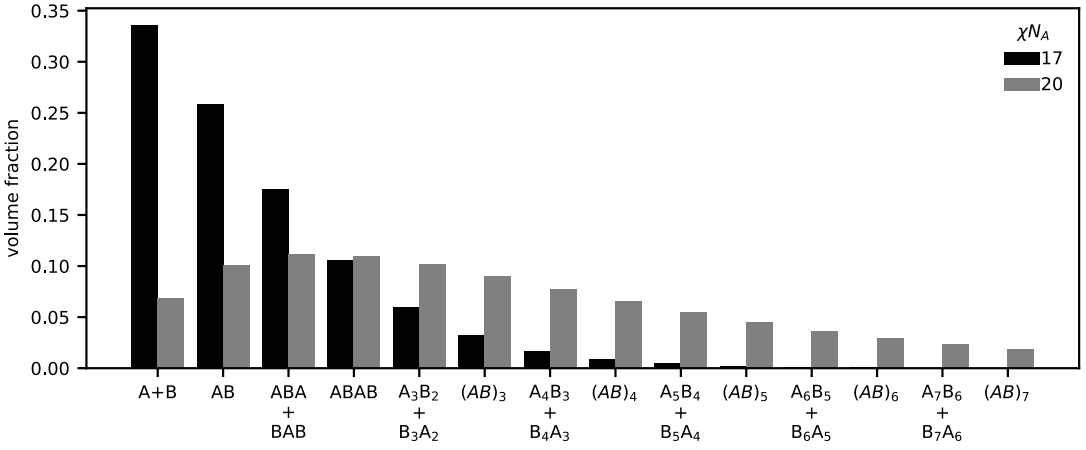

Figure 4. Distribution of products in the lamellar phase at $h/\chi N_A = 0.5$, $\psi_A = 0.5$, and $\chi N_A = 17$ or $\chi N_A = 20$. Blend is self-assembled into LAM at both $\chi N_A = 17$ and 20.

https://doi.org/10.1021/acs.macromol.3c01653
Macromolecules 2023, 56, 9994−10005

order−disorder transition (ODT) is also quite different from unreactive BCPs and has a cusp in the center of the phase diagram, indicating that at $\psi_A = 0.5$, the mixture has a higher segregation strength χN_{ODT} at the ODT than at $\psi_A = 0.33$ or $\psi_A = 0.66$.

Figure 5 also shows the spinodal boundary computed via the random phase approximation (RPA)[3,32] in red. The dashed segments of the red line indicate nonzero wave vector k instability, which is characteristic of microphase separation. The solid section of the red line indicates a wave vector $k = 0$ instability, indicative of phase coexistence and possible macroscopic phase separation. The RPA is in good agreement with the full phase diagram from SCFT. The dashed segments of the RPA boundary, which indicate microphase separation, lie within the single-phase regions of the phase diagram. RPA also predicts a change from $k \neq 0$ to $k = 0$ instability near the BCC-HEX-DIS triple point at $\chi N_A = 10.5$. The solid section of the RPA line, which indicates macrophase separation, lies inside the DIS-HEX coexistence region. We now examine the reaction equilibrium and then explain the shape of the ODT.

Figure 6 shows the conversion of species A with varying χN_A at $\psi_A = 0.5$, analogous to Figure 2 for weak bonding. For strong

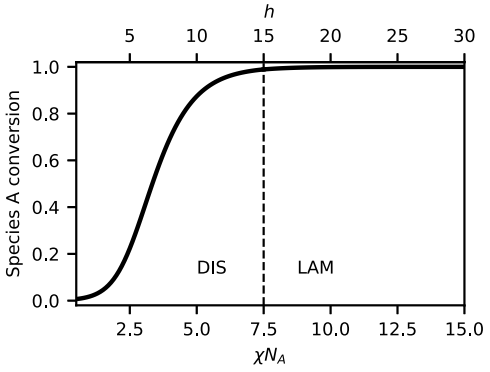

Figure 6. Species A conversion, α_A, versus χN_A at $h/\chi N_A = 2.0$ and $\psi_A = 0.5$. Text labels the stable phase and the vertical dashed line indicates the phase boundary.

bonding, the conversion of species A increases quite quickly with increasing χN_A so that at $\chi N_A = 2$ (the unreactive homopolymer blend critical point), $\alpha_A = 0.1$. At this level of conversion, there is enough BCP present to compatibilize the A and B homopolymers and maintain a single disordered phase despite the relatively strong χN_A. Further increasing χN_A continues to increase the conversion until it reaches near completion. Near the ODT at $\chi N_A = 7.45$, the conversion in the disordered phase reached nearly 100%. Crossing into the lamellar phase continues this trajectory and the conversion stays near unity. One can repeat this exercise at other values of ψ_A to find that the minority species is nearly 100% converted at the ODT for all compositions.

Based on this information, we might approximate the system as being composed of all BCPs or copolymers plus a single excess homopolymer component, depending on stoichiometry. Using this assumption, we can rationalize the shape of the ODT based on the stoichiometry of the system. For $\psi_A = 0.5$, stoichiometry allows for $\alpha = 1$ for both species, so that extremely long AB repeating BCPs can be formed. At $\psi_A = 2/3$, the stoichiometry would allow for the formation of all ABA triblocks as there are two A chains present for each B chain. At $\psi_A = 1/3$, the inverse is true, allowing the formation of all BAB triblocks. Finally, at $\psi_A = 0$ and $\psi_A = 1$, the system is composed entirely of a B or A homopolymer, respectively. We can then approximate various parts of the ODT envelope using mixtures of these different components. In Figure 7, we use RPA to plot

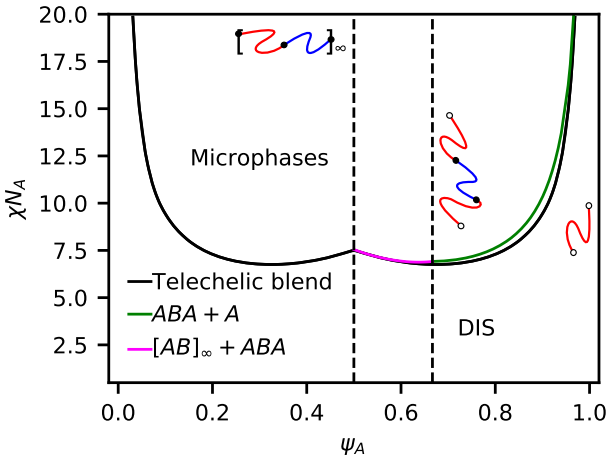

Figure 7. Order−disorder spinodals computed via RPA for the telechelic blend system at $h/\chi N_A = 2$ (black), an unreactive binary blend of ABA triblock and A homopolymer (green), and an unreactive blend of ABA triblock with infinitely repeating (AB) multiblock (magenta).

the disordered phase spinodal boundary (above or coincident with the ODT) for the fully reactive telechelic blend as well as for binary blends of homopolymers, triblocks, and the AB repeating polymer.

The unreactive binary blends match reasonably closely to the fully reactive telechelic system. This is somewhat surprising because the telechelic system is composed of a wide array of different BCP products. In Figure 8, we plot the full

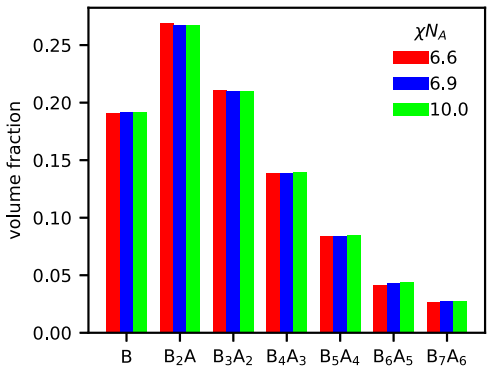

Figure 8. Distribution of products found in the telechelic blend at $\psi_A = 0.32$, $h/\chi N_A = 2$, and various χN_A. For $\chi N_A = 6.6$, the blend forms a homogeneous disordered phase. For $\chi N_A = 6.9$ or 10.0, the blend self-assembles into HEX.

distribution of products at $\psi_A = 0.32$ and $\chi N_A = 6.6$, 6.9, or 10.0. At $\chi N_A = 6.6$, the system is still in the disordered phase, whereas at the two higher χN_A values, the HEX phase is stable. In all cases, triblock polymers make up less than 30% of the volume, despite the stoichiometry allowing for the near-complete formation of triblocks. Homopolymers remain a significant contribution at ≈19% of the volume, and higher-order BCPs that are B-terminated make up the remainder. Although the crude model of a triblock mixed with a

https://doi.org/10.1021/acs.macromol.3c01653
Macromolecules 2023, 56, 9994−10005

homopolymer matches the ODT for the telechelic blend closely, it does not represent the actual distribution of products.

We are also able to evaluate the distribution of products at $\psi_A = 0.5$ and $\chi N_A = 7$, which is just below the ODT. Considering products with a length of up to 50 telechelics accounts for only 25% of the mass in the system, which reveals that the system is dominated by very long BCPs.

As a final comparison to the weak-bonding case, we plot the domain spacing of the lamellar phase at $\psi_A = 0.5$, as shown in Figure 9. For high bond strength, the domain spacing increases

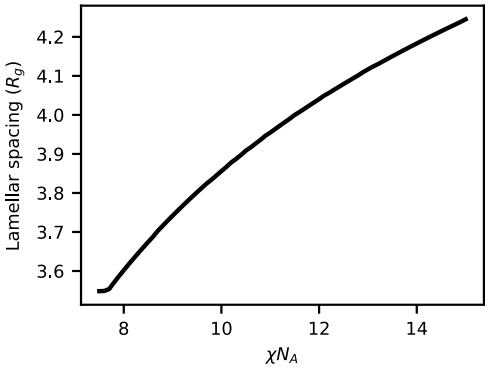

Figure 9. Domain spacing of the lamellar phase as a function of χN_A at $h/\chi N_A = 2.0$ and $\psi_A = 0.5$.

with increasing χN_A, which is the opposite trend that occurs at weak bonding. Additionally, the magnitude of change in domain spacing is much smaller at strong bonding compared to weak bonding. We can attribute the difference between the two regimes to the mechanisms that cause the domain spacing to change. At weak bonding, the domain size was largely affected by the conversion in the system and the amount of unreacted homopolymer that was present to swell the system. At strong bonding, the conversion is nearly unity in the lamellar phase, as shown in Figure 6. This means there is little to no homopolymer present to swell the system and the previous mechanism is no longer relevant. Instead, the brush physics at the lamellar interface dominate. In this picture, as χN_A increases, the chains stretch away from the interface to reduce the interfacial area per unit volume, leading to increased domain spacing.[51]

Intermediate Bonding. Thus far, we have considered supramolecular bonds that are relatively strong or weak compared to segregation strength. We now consider the transition between the two regimes and examine an intermediate bond strength of $h/\chi N_A = 1.5$, for which the phase diagram is illustrated in Figure 10. The phase diagram shows features from both the weak bonding and strong bonding phase portraits. For $2 < \chi N_A < 3.6$, it is possible to phase separate into two DIS phases, similar to the weak-bonding case. This region has both UCST and LCST character and closes for $\chi N_A > 3.6$, where a single DIS becomes stable. As χN_A is further increased, the system undergoes another transition, but this time into microphases. We do not perform a full numerical SCFT investigation of this region, but the RPA reveals that the disordered phase has instabilities at nonzero wave vector k, indicating the formation of microphases. Furthermore, the shape of the phase boundary is highly reminiscent of that from $h/\chi N_A = 2$ and we expect very similar stability windows. Such rich and reentrant phase behavior in

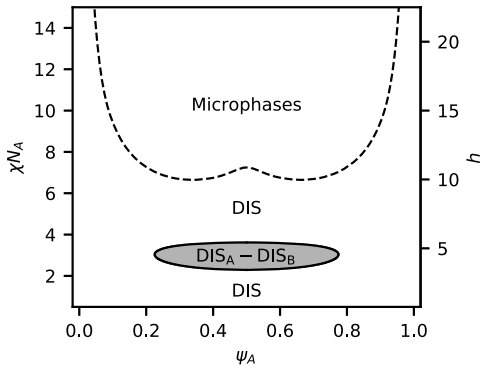

Figure 10. Phase diagram for a binary blend of heterobonding telechelic homopolymers at $h/\chi N_A = 1.5$. Shaded regions indicate two-phase coexistence, while white regions indicate a single-phase is present. Only the stability limit of the homogeneous DIS phase to microphases is shown by the RPA analysis.

the intermediate bonding strength regime was previously identified by RPA analysis of the binary telechelic system.[52]

To understand this complex phase portrait, we again turn to the reaction equilibrium. Figure 11 shows the conversion of

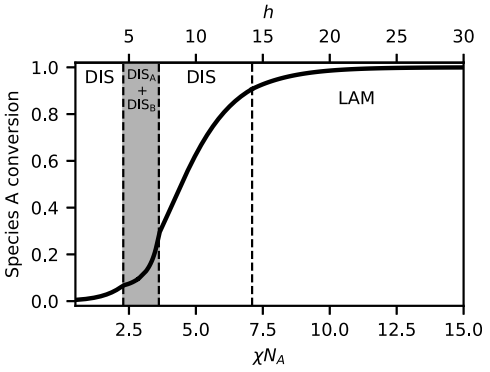

Figure 11. Species A conversion, α_A, versus χN_A (solid dark line) at $h/\chi N_A = 1.5$ and $\psi_A = 0.5$. Shading and text labels indicate the stable phase(s). Vertical dashed lines indicate phase boundaries.

species A at $\psi_A = 0.5$ for varying χN_A. As in previous cases, conversion increases with increasing χN_A. At $\chi N_A \approx 2.25$, the conversion of species A is $\alpha_A \approx 0.07$, corresponding to an approximately 10% volume fraction of copolymer. This is an insufficient quantity of copolymer to prevent phase separation, but it is enough to delay phase separation from the unreactive critical point of $\chi N_A = 2$. As χN_A is further increased above 2.25, the conversion continues to increase, in contrast to the weak-bonding case, where conversion started to decrease upon phase separation. In this intermediate bonding case, the phase segregation near the critical point is weak and the A-rich phase is composed of at least 20% component B. The equilibrium constant is also sufficiently large so that forming BCP products is still favored, and conversion continues to increase. A careful examination of the conversion reveals that the phase separation does slightly depress conversion compared to a hypothetical scenario of a well-mixed single phase, but this effect is rather weak.

As χN_A is increased through the two-phase window, eventually enough copolymer is formed to recompatibilize the two phases at $\chi N_A \approx 3.6$. The conversion at this point is $\alpha_A \approx 0.27$, which corresponds to a combined homopolymer

https://doi.org/10.1021/acs.macromol.3c01653
Macromolecules 2023, 56, 9994−10005

volume fraction of 52%. This is consistent with previous theoretical studies of A homopolymer + B homopolymer + AB diblock that found that approximately 45% volume fraction of diblock copolymer was sufficient to compatibilize homopolymers[53] when the homopolymer had half the length of the diblock, as in this study. For $\chi N_A > 3.6$, the conversion plot strongly resembles that of the strong bonding case, and eventually the blend self-assembles into a lamellar phase. The trends in lamellar domain spacing also mimic those of the strong bonding case, and domain spacing increases monotonically with increasing χN_A.

The phase behavior at this intermediate value of $h/\chi N_A$ is indicative of being near a Lifshitz tricritical point, where microphase separation, macrophase separation, and a single disordered phase meet at a single point. It is known from unreactive polymer blends that SCFT fails dramatically near the Lifshitz point and fluctuations stabilize bicontinuous microemulsions.[54−56] We expect such fluctuations to also be present in this system, but we do not speculate further on their effects. In principle, it is possible to include fluctuation effects in our model via field-theoretic simulations, which would also include cyclic copolymer species, but we defer such efforts to future work.

Unequal Telechelic Polymer Lengths. Up to this point, we have only considered blends where the two telechelic homopolymers are of equal length. We next consider the case where the B telechelic is half as long as the A homopolymer, $N_B/N_A = 0.5$. Upon breaking the molar mass symmetry of the two polymers,the compositional symmetry of the phase diagram is correspondingly broken. Figure 12 shows the

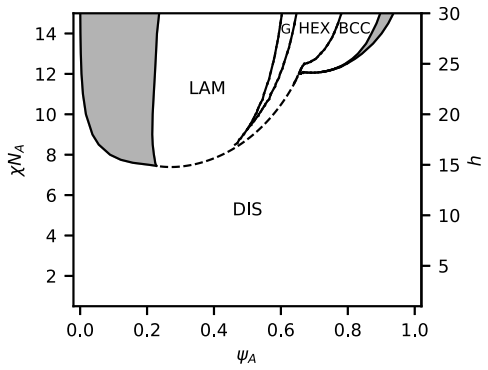

Figure 12. Phase diagram for a binary blend of heterobonding telechelic homopolymers at $h/\chi N_A = 2$ with $N_B/N_A = 0.5$. Shaded regions indicate two-phase coexistence, while white regions indicate a single-phase is present. Dashed line indicates the RPA spinodal boundary.

phase diagram for $N_B/N_A = 0.5$ and $h/\chi N_A = 2$. The phase diagram is dominated by the lamellar phase, which is stable as a pure phase or in coexistence with a disordered phase for $\psi_A < 0.5$. This is to be expected, as the analogous unreactive system consists of a BAB triblock that has an equal number of total A and B segments, blended with a B homopolymer. A similar system of symmetric AB diblock blended with B homopolymer also produced a region of LAM stability as well as LAM and DIS coexistence.[46,57] For $\psi_A > 0.5$, other phases form, including GYR, HEX, and BCC. We do not include coexistence regions between microphases but rather draw solid lines where the free energies of the two phases cross. Coexistence regions between microphases have widths less than 0.01.

The asymmetric two-lobe structure of the phase diagram can also be understood by a comparison with unreactive analogous. The cusp occurs at $\phi_A = 2/3$, which is the stoichiometric composition to form repeating AB BCPs. Figure 13 compares

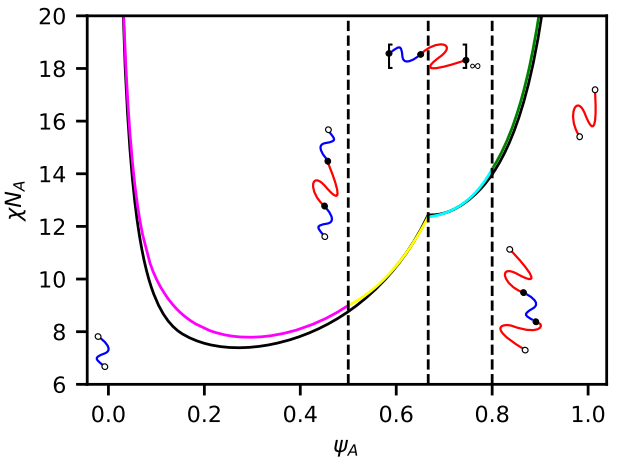

Figure 13. Order−disorder spinodal boundaries computed via RPA for the telechelic blend system with $N_B/N_A = 0.5$ (black) and multiple unreactive binary blends, including: ABA triblock and A homopolymer (green), ABA triblock with infinitely repeating (AB) multiblock (cyan), BAB triblock with infinitely repeating (AB) multiblock (yellow), and BAB triblock with B homopolymer (magenta).

the telechelic blend spinodal boundary to that of various unreactive blends similar to that in Figure 7. Note, however, that the actual distribution of products is likely significantly different than the unreactive analogous considered here. This point was demonstrated earlier for equal length telechelic homopolymers.

COMPARISON WITH EXPERIMENTS

One of the earliest experimental investigations of the phase behavior of telechelic blends is due to Russell and co-workers.[9] They used small-angle X-ray scattering to study blends of telechelic polyisoprene and polystyrene that were end-functionalized with amino and acid groups, respectively. The acid groups considered were carboxylic and sulfonic acids. Supramolecular bonds can form when an acid protonates an amino group, which induces an ionic bond. Bulk polyisoprene and polystyrene have dielectric constants near 3, so it is very unfavorable for unpaired ions to exist. For the bonds to dissociate, the reverse proton transfer must occur so that the neutral amine and acid can separate from one another. Evidence for the partial conversion of acid and base to paired ions was found by FT-IR in later work by Iwasaki and co-workers.[22]

The scattering data from amino-terminated polyisoprene blended with carboxylic acid-terminated polystyrene are consistent with the weak-bonding picture presented in this work. The authors observed microphase formation at low temperatures (high χ) and that upon heating, the blend would undergo spinodal decomposition and macroscopically phase separation, analogous to decreasing χN_A in Figure 1. Additionally, the domain size of the microphase was found to significantly increase with increasing temperature (decreasing χN_A), consistent with weak-bonding domain size trends, as

https://doi.org/10.1021/acs.macromol.3c01653
Macromolecules 2023, 56, 9994−10005

shown in Figure 3. The authors showed that the change in domain size was too large to be attributed to thermal expansion; therefore, the change in domain size due to homopolymer swelling demonstrated in this work may play a role.

When the carboxylic acid groups were replaced with sulfonic acid groups, Russell and co-workers found qualitatively different behavior. The blend again formed a microphase at low temperature, but upon heating, it became disordered rather than undergoing spinodal decomposition. This is consistent with the strong-bonding phase behavior presented in Figure 5. Additionally, the domain spacing of the microphase had a much weaker dependence on temperature compared with the blend with carboxylic acid. The domain size slightly decreased with increasing temperature, consistent with the trends in domain size at strong bonding in Figure 9. The blend with sulfonic-acid-functionalized polystyrene thus behaves like a polymer in the strong bonding regime predicted in this work. Furthermore, sulfonic acid is a stronger acid than carboxylic acid; therefore, the effective equilibrium constant should be larger for the sulfonic acid-amine pairing. Finally, Russell and coauthors showed that if the length of the polystyrene polymers was increased, then the system would again macrophase separate at high temperature, consistent with the intermediate-bonding phase diagram in Figure 10. This is consistent with previous theoretical investigations that showed that increased polymer length dilutes the concentration of end groups and leads to an effectively weaker equilibrium constant.[26]

There have been multiple subsequent reports that utilize the same acid-amine chemistry as Russell and co-workers, but swap the isoprene monomer with a different chemical species, including ethylene oxide, isobutylene, and dimethylsiloxane.[22,58,59] In addition to SAXS, these authors have performed FT-IR, proton NMR, TEM, and rheological measurements on their samples to provide further evidence for BCP formation from the starting homopolymers and the presence of an ODT. One group of authors was also able to estimate the approximate values of χN_A for which the ODT occurs, which matches closely to the value we predict at equal composition, as shown in Figure 5.[58] In all of the referenced papers except those by Russell and co-workers, only equimolar blends of telechelic polymers were considered, so much of the phase space remains unexplored.

In addition to the acid base supramolecular interactions, there have been investigations of telechelic polymers that interact through hydrogen bonding.[60,61] These investigations are not as extensive as the previously discussed work but were able to show evidence of microphase formation via SAXS and TEM. Unfortunately, there is not enough temperature-dependent data to compare these works with the bonding strength cases considered here.

CONCLUSIONS

We have demonstrated that a wide variety of phase behaviors can be achieved with binary blends of heterobonding telechelic homopolymers. By properly tuning the relative strength of the bonding equilibrium constant to the segregation strength, it is possible to make the system behave like an unreactive homopolymer blend or a BCP melt. Although some of the microphase stability windows have unconventional shapes, these stability windows can be rationalized by considering the stoichiometry of the system. Additionally, the microphases that are formed from the telechelic blend can have highly variable domain sizes and differing dependence on temperature, depending on the relative strength of bonding and phase separation. The models presented here are able to quantitatively predict all of these phenomena and are consistent with previous experiments. This work confirms that CS-SCFT is a powerful theoretical and computational framework that can further guide the experimental investigation of supramolecular blends.

AUTHOR INFORMATION

Corresponding Author

Glenn H. Fredrickson − *Department of Chemical Engineering, University of California, Santa Barbara, California 93106, United States; Materials Research Laboratory, University of California, Santa Barbara, California 93106, United States;* orcid.org/0000-0002-6716-9017; Email: ghf@mrl.ucsb.edu

Authors

Daniel L. Vigil − *Department of Chemical Engineering, University of California, Santa Barbara, California 93106, United States;* orcid.org/0000-0001-9860-0888

Amy Zhang − *Department of Chemical Engineering, University of California, Santa Barbara, California 93106, United States*

Kris T. Delaney − *Materials Research Laboratory, University of California, Santa Barbara, California 93106, United States;* orcid.org/0000-0003-0356-1391

Complete contact information is available at: https://pubs.acs.org/10.1021/acs.macromol.3c01653

Notes

The authors declare no competing financial interest.

ACKNOWLEDGMENTS

The authors acknowledge support from the NSF Graduate Research Fellowship Program under grant no. 1650114 and the NSF CMMT Program under grant no. DMR-2104255. Use was made of computational facilities purchased with funds from the NSF (grant no. OAC-1925717) and administered by the Center for Scientific Computing (CSC). The CSC is supported by the California NanoSystems Institute and the Materials Research Science and Engineering Center (MRSEC; NSF grant no. DMR 1720256) at UC Santa Barbara. Any opinions, findings, and conclusions or recommendations expressed in this material are those of the authors and do not necessarily reflect the views of the NSF.

REFERENCES

(1) Huggins, M. L. Solutions of Long Chain Compounds. *J. Chem. Phys.* **1941**, *9*, 440−441.
(2) Flory, P. J. Thermodynamics of High Polymer Solutions. *J. Chem. Phys.* **1942**, *10*, 51−61.
(3) Leibler, L. Theory of Microphase Separation in Block Copolymers. *Macromolecules* **1980**, *13*, 1602−1617.
(4) Matsen, M. W.; Schick, M. Stable and Unstable Phases of a Diblock Copolymer Melt. *Phys. Rev. Lett.* **1994**, *72*, 2660−2663.
(5) Grason, G. M.; DiDonna, B. A.; Kamien, R. D. Geometric Theory of Diblock Copolymer Phases. *Phys. Rev. Lett.* **2003**, *91*, 058304.
(6) Xie, N.; Li, W.; Qiu, F.; Shi, A.-C. σ Phase Formed in Conformationally Asymmetric AB-Type Block Copolymers. *ACS Macro Lett.* **2014**, *3*, 906−910.

https://doi.org/10.1021/acs.macromol.3c01653
Macromolecules 2023, 56, 9994−10005

(7) Fredrickson, G. H. *The Equilibrium Theory of Inhomogeneous Polymers*. International Series of Monographs on Physics; Clarendon Press: Oxford, New York, England, 2006; p 134.
(8) Harmon, T. S.; Holehouse, A. S.; Rosen, M. K.; Pappu, R. V. Intrinsically disordered linkers determine the interplay between phase separation and gelation in multivalent proteins. *eLife* **2017**, *6*, No. e30294.
(9) Russell, T. P.; Jerome, R.; Charlier, P.; Foucart, M. The microstructure of block copolymers formed via ionic interactions. *Macromolecules* **1988**, *21*, 1709−1717.
(10) Huh, J.; Park, H.; Kim, K.; Kim, K.; Park, C.; Jo, W. Giant Thermal Tunability of the Lamellar Spacing in Block-Copolymer-Like Supramolecules Formed from Binary-End-Functionalized Polymer Blends. *Adv. Mater.* **2006**, *18*, 624−629.
(11) Feldman, K. E.; Kade, M. J.; Meijer, E. W.; Hawker, C. J.; Kramer, E. J. Phase Behavior of Complementary Multiply Hydrogen Bonded End-Functional Polymer Blends. *Macromolecules* **2010**, *43*, 5121−5127.
(12) Yount, W. C.; Loveless, D. M.; Craig, S. L. Small-Molecule Dynamics and Mechanisms Underlying the Macroscopic Mechanical Properties of Coordinatively Cross-Linked Polymer Networks. *J. Am. Chem. Soc.* **2005**, *127*, 14488−14496. PMID: 16218645
(13) Koberstein, J. T.; Gancarz, I.; Clarke, T. C. The effects of morphological transitions on hydrogen bonding in polyurethanes: Preliminary results of simultaneous DSC−FTIR experiments. *J. Polym. Sci., Part B: Polym. Phys.* **1986**, *24*, 2487−2498.
(14) Yang, W.; Macosko, C.; Wellinghoff, S. Thermal degradation of urethanes based on 4,4'-diphenylmethane diisocyanate and 1,4-butanediol (MDI/BDO). *Polymer* **1986**, *27*, 1235−1240.
(15) Martin, D. J.; Meijs, G. F.; Gunatillake, P. A.; McCarthy, S. J.; Renwick, G. M. The effect of average soft segment length on morphology and properties of a series of polyurethane elastomers. II. SAXS-DSC annealing study. *J. Appl. Polym. Sci.* **1997**, *64*, 803−817.
(16) Ruokolainen, J.; Mäkinen, R.; Torkkeli, M.; Mäkelä, T.; Serimaa, R.; Brinke, G. t.; Ikkala, O. Switching Supramolecular Polymeric Materials with Multiple Length Scales. *Science* **1998**, *280*, 557−560.
(17) Cordier, P.; Tournilhac, F.; Soulié-Ziakovic, C.; Leibler, L. Self-healing and thermoreversible rubber from supramolecular assembly. *Nature* **2008**, *451*, 977−980.
(18) Rumyantsev, A. M.; Kramarenko, E. Y. Two regions of microphase separation in ion-containing polymer solutions. *Soft Matter* **2017**, *13*, 6831−6844.
(19) Kulshreshtha, A.; Jayaraman, A. Phase Behavior and Morphology of Blends Containing Associating Polymers: Insights from Liquid-State Theory and Molecular Simulations. *Macromolecules* **2022**, *55*, 9297−9311.
(20) Danielsen, S. P. O. Chemical Compatibilization, Macro-and Microphase Separation of Heteroassociative Polymers. *Macromolecules* **2023**, *56*, 6527−6542.
(21) Danielsen, S. P. O.; Semenov, A. N.; Rubinstein, M. Phase Separation and Gelation in Solutions and Blends of Heteroassociative Polymers. *Macromolecules* **2023**, *56*, 5661−5677.
(22) Iwasaki, K.; Hirao, A.; Nakahama, S. Morphology of blends of α, ω-diaminopolystyrene with α, ω-dicarboxypoly(ethylene oxide). *Macromolecules* **1993**, *26*, 2126−2131.
(23) Vukovic, I.; Voortman, T. P.; Merino, D. H.; Portale, G.; Hiekkataipale, P.; Ruokolainen, J.; ten Brinke, G.; Loos, K. Double Gyroid Network Morphology in Supramolecular Diblock Copolymer Complexes. *Macromolecules* **2012**, *45*, 3503−3512.
(24) Vukovic, I.; ten Brinke, G.; Loos, K. Hexagonally Perforated Layer Morphology in PS-b-P4VP(DPP) Supramolecules. *Macromolecules* **2012**, *45*, 9409−9418.
(25) Huh, J.; Jo, W. H. Theory on Phase Behavior of Triblocklike Supramolecules Formed from Reversibly Associating End-functionalized Polymer Blends. *Macromolecules* **2004**, *37*, 3037−3048.
(26) Feng, E. H.; Lee, W. B.; Fredrickson, G. H. Supramolecular Diblock Copolymers: A Field-Theoretic Model and Mean-Field Solution. *Macromolecules* **2007**, *40*, 693−702.
(27) Lee, W. B.; Elliott, R.; Katsov, K.; Fredrickson, G. H. Phase Morphologies in Reversibly Bonding Supramolecular Triblock Copolymer Blends. *Macromolecules* **2007**, *40*, 8445−8454.
(28) Mohan, A.; Elliot, R.; Fredrickson, G. H. Field-theoretic model of inhomogeneous supramolecular polymer networks and gels. *J. Chem. Phys.* **2010**, *133*, 174903.
(29) Mester, Z.; Mohan, A.; Fredrickson, G. H. Macro- and Microphase Separation in Multifunctional Supramolecular Polymer Networks. *Macromolecules* **2011**, *44*, 9411−9423.
(30) Man, X.; Delaney, K. T.; Villet, M. C.; Orland, H.; Fredrickson, G. H. Coherent States Formulation of Polymer Field Theory. *J. Chem. Phys.* **2014**, *140*, 024905.
(31) Fredrickson, G. H. *Field-Theoretic Simulations in Soft Matter and Quantum Fluids; International Series of Monographs on Physics*; Oxford University Press: Oxford, 2023; Vol. *173*.
(32) Fredrickson, G. H.; Delaney, K. T. Coherent States Field Theory in Supramolecular Polymer Physics. *J. Chem. Phys.* **2018**, *148*, 204904.
(33) Vigil, D. L.; García-Cervera, C. J.; Delaney, K. T.; Fredrickson, G. H. Linear Scaling Self-Consistent Field Theory with Spectral Contour Accuracy. *ACS Macro Lett.* **2019**, *8*, 1402−1406.
(34) Amit, D. J. *Field Theory, the Renormalization Group and Critical Phenomena*, 2nd ed.; World Scientific, 1993.
(35) Fredrickson, G. H.; Delaney, K. T. Direct free energy evaluation of classical and quantum many-body systems via field-theoretic simulation. *Proc. Natl. Acad. Sci. U.S.A.* **2022**, *119*, No. e2201804119.
(36) Barrat, J.-L.; Fredrickson, G. H.; Sides, S. W. Introducing Variable Cell Shape Methods in Field Theory Simulations of Polymers. *J. Phys. Chem. B* **2005**, *109*, 6694−6700. PMID: 16851752
(37) Janert, P. K.; Schick, M. Phase Behavior of Ternary Homopolymer/Diblock Blends: Influence of Relative Chain Lengths. *Macromolecules* **1997**, *30*, 137−144.
(38) Spencer, R. K. W.; Matsen, M. W. Fluctuation effects in blends of A + B homopolymers with AB diblock copolymer. *J. Chem. Phys.* **2018**, *148*, 204907.
(39) Vorselaars, B.; Spencer, R. K. W.; Matsen, M. W. Instability of the Microemulsion Channel in Block Copolymer-Homopolymer Blends. *Phys. Rev. Lett.* **2020**, *125*, 117801.
(40) Spencer, R. K. W.; Matsen, M. W. Coexistence of Polymeric Microemulsion with Homopolymer-Rich Phases. *Macromolecules* **2021**, *54*, 1329−1337.
(41) Panagiotopoulos, A. Z. Direct determination of phase coexistence properties of fluids by Monte Carlo simulation in a new ensemble. *Mol. Phys.* **1987**, *61*, 813−826.
(42) Panagiotopoulos, A.; Quirke, N.; Stapleton, M.; Tildesley, D. Phase equilibria by simulation in the Gibbs ensemble. *Mol. Phys.* **1988**, *63*, 527−545.
(43) Riggleman, R. A.; Fredrickson, G. H. Field-theoretic simulations in the Gibbs ensemble. *J. Chem. Phys.* **2010**, *132*, 024104.
(44) Mester, Z.; Lynd, N. A.; Fredrickson, G. H. Numerical self-consistent field theory of multicomponent polymer blends in the Gibbs ensemble. *Soft Matter* **2013**, *9*, 11288−11294.
(45) Mester, Z.; Lynd, N. A.; Delaney, K. T.; Fredrickson, G. H. Phase Coexistence Calculations of Reversibly Bonded Block Copolymers: A Unit Cell Gibbs Ensemble Approach. *Macromolecules* **2014**, *47*, 1865−1874.
(46) Matsen, M. W. Phase Behavior of Block Copolymer/Homopolymer Blends. *Macromolecules* **1995**, *28*, 5765−5773.
(47) Helfrich, W. Steric Interaction of Fluid Membranes in Multilayer Systems. *Z. Naturforsch.* **1978**, *33*, 305−315.
(48) Milner, S.; Roux, D. Flory theory of the unbinding transition. *J. Phys.* **1992**, *2*, 1741−1754.
(49) Kim, J. U.; Yang, Y.-B.; Lee, W. B. Self-Consistent Field Theory of Gaussian Ring Polymers. *Macromolecules* **2012**, *45*, 3263−3269.
(50) Grest, G. S.; Ge, T.; Plimpton, S. J.; Rubinstein, M.; O'Connor, T. C. Entropic Mixing of Ring/Linear Polymer Blends. *ACS Polym. Au* **2023**, *3*, 209−216.
(51) Bates, F. S.; Fredrickson, G. H. Block Copolymers-Designer Soft Materials. *Phys. Today* **1999**, *52*, 32−38.

https://doi.org/10.1021/acs.macromol.3c01653
Macromolecules 2023, 56, 9994−10005

(52) Elliott, R.; Fredrickson, G. H. Supramolecular assembly in telechelic polymer blends. *J. Chem. Phys.* **2009**, *131*, 144906.
(53) Broseta, D.; Fredrickson, G. H. Phase equilibria in copolymer/homopolymer ternary blends: Molecular weight effects. *J. Chem. Phys.* **1990**, *93*, 2927−2938.
(54) Bates, F. S.; Maurer, W. W.; Lipic, P. M.; Hillmyer, M. A.; Almdal, K.; Mortensen, K.; Fredrickson, G. H.; Lodge, T. P. Polymeric Bicontinuous Microemulsions. *Phys. Rev. Lett.* **1997**, *79*, 849−852.
(55) Düchs, D.; Ganesan, V.; Fredrickson, G. H.; Schmid, F. Fluctuation Effects in Ternary AB + A + B Polymeric Emulsions. *Macromolecules* **2003**, *36*, 9237−9248.
(56) Vorselaars, B.; Spencer, R. K. W.; Matsen, M. W. Instability of the Microemulsion Channel in Block Copolymer-Homopolymer Blends. *Phys. Rev. Lett.* **2020**, *125*, 117801.
(57) Matsen, M. W. New Fast SCFT Algorithm Applied to Binary Diblock Copolymer/Homopolymer Blends. *Macromolecules* **2003**, *36*, 9647−9657.
(58) Zhang, L.; Kucera, L. R.; Ummadisetty, S.; Nykaza, J. R.; Elabd, Y. A.; Storey, R. F.; Cavicchi, K. A.; Weiss, R. A. Supramolecular Multiblock Polystyrene-Polyisobutylene Copolymers via Ionic Interactions. *Macromolecules* **2014**, *47*, 4387−4396.
(59) Güillen Obando, A.; Chen, Y.; Qiang, Z. A simple route to prepare supramolecular block copolymers using telechelic polystyrene/polydimethylsiloxane pairs. *Polym. Int.* **2022**, *71*, 470−477.
(60) Binder, W. H.; Kunz, M. J.; Ingolic, E. Supramolecular poly(ether ketone)-polyisobutylene pseudo-block copolymers. *J. Polym. Sci., Part A: Polym. Chem.* **2004**, *42*, 162−172.
(61) Gooch, A.; Nedolisa, C.; Houton, K. A.; Lindsay, C. I.; Saiani, A.; Wilson, A. J. Tunable Self-Assembled Elastomers Using Triply Hydrogen-Bonded Arrays. *Macromolecules* **2012**, *45*, 4723−4729.

https://doi.org/10.1021/acs.macromol.3c01653
Macromolecules 2023, 56, 9994−10005